

White Dwarf–White Dwarf collisions in AGN discs via close encounters

Yan Luo,^{1,2}* Xiao-Jun Wu,^{1,2} Shu-Rui Zhang,^{1,2} Jian-Min Wang,³ Luis C. Ho,⁴ Ye-Fei Yuan^{1,2}†

¹*School of Astronomy and Space Science, University of Science and Technology of China, Hefei 230026, China*

²*CAS Key Laboratory for Research in Galaxies and Cosmology, Department of Astronomy, University of Science and Technology of China, Hefei 230026, China*

³*Key Laboratory for Particle Astrophysics, Institute of High Energy Physics, Chinese Academy of Sciences, 19B Yuquan Road, Beijing 100049, China*

⁴*Kavli Institute for Astronomy and Astrophysics, Peking University, Beijing 100871, China*

Accepted 2023 July 18. Received 2023 June 24; in original form 2022 September 30

ABSTRACT

White dwarfs (WDs) in active galactic nucleus (AGNs) discs might migrate to the inner radii of the discs and form restricted three-body systems with two WDs moving around the central supermassive black hole (SMBH) in close orbits. These systems could be dynamical unstable, which can lead to very close encounters or direct collisions. In this work, we use N-body simulations to study the evolution of such systems with the different initial orbital separation p , relative orbital inclination Δi and SMBH mass M . It is found that the close encounters of WDs mainly occur at $1.1R_H \lesssim p \lesssim 2\sqrt{3}R_H$, where R_H is the mutual Hill radius. For $p < 1.1R_H$, the majority of WDs move in horseshoe or tadpole orbits, and only few of them with small initial orbital phase difference undergo close encounters. For $p = 3.0R_H$, WD-WD collisions occur in most of the samples within a time of $10^5 P_1$, and considerable collisions occur within a time of $t < 62 P_1$ for small orbital radii, where P_1 is the orbital period. The peak of the closest separation distribution increase and the WD-WD collision fraction decreases with an increase of the relative inclination. The closest separation distribution is similar in cases with the different SMBH mass, but the WD-WD collision fraction decreases as the mass of SMBHs increases. According to our estimation, the event rate of the cosmic WD-WD collision in AGN discs is about $300\text{Gpc}^{-3}\text{yr}^{-1}$, roughly 1% of the one of the observed type Ia supernova. The corresponding electromagnetic emission signals can be observed by large surveys of AGNs.

Key words: accretion, accretion disc - binaries: general - stars: white dwarfs - dynamical evolution: collision - supernovae - method: numerical

1 INTRODUCTION

Active galactic nuclei (AGNs) are considered to be an important astrophysics environment for mergers and collisions of binary compact objects and gravitational wave events (Cheng & Wang 1999), and have recently been the subject of renewed interest (Tagawa et al. 2020a; McKernan et al. 2020a,b; Li 2022; McKernan et al. 2018; Li & Lai 2022; Bartos et al. 2017). Due to their deep potential and high gas density, AGNs can retain a large population of stellar remnants and lead to hierarchical merger (Yang et al. 2019a; Tagawa et al. 2020b; Wang et al. 2021a; Liu & Lai 2021). These compact objects are probably derived from nuclear star clusters or stellar evolution in situ in the extended region ($\sim \text{pc}$) of the AGN discs (Stone et al. 2017; Dittmann & Miller 2020). In this environment, compact objects may be captured and align with the AGN discs. (Yang et al. 2019b). Tanaka et al. (2002); Paardekooper et al. (2010); McKernan et al. (2012) indicate that the torque exerted by the disc helps them move to the migration trap (Bellovary et al. 2016; Secunda et al. 2019; Secunda et al. 2020) within the disc. Normally, the migration traps are located around 20 – 300 Schwarzschild radius. Thus, It is not unreasonable to expect that many of these compact objects will be assembled in the AGN discs, which could be responsible for some LIGO/Virgo

black hole (BH) binary merger events. Due to high gas density, these compact objects accrete gas in AGN discs (Pan & Yang 2021; Wang et al. 2021b), and mergers of these compact objects may potentially be associated with some electromagnetic radiation (Cheng & Wang 1999; Wang et al. 2021c).

Following the LIGO/Virgo collaborations (Abbott et al. 2019, 2021; The LIGO Scientific Collaboration et al. 2021), BH-BH mergers in AGN discs have attracted much attention (Gayathri et al. 2021; Samsing et al. 2020; Fabj et al. 2020; Tagawa et al. 2021a; Gröbner et al. 2020). In the AGN discs, the enrichment of compact objects enhances the mergers between compact objects. The initial mass function (IMF) (Kroupa 2001) suggests that there are more neutron stars (NSs) and white dwarfs (WDs) than BHs exist in the AGN discs. These high-density WDs within the disc might lead to tidal disruption of WD by BH (Haas et al. 2012; Anninos et al. 2018; Kawana et al. 2018; Fragione et al. 2018) and supernovae due to the merger of WDs (Kashyap et al. 2018; Ji et al. 2013). As a result, the associated electromagnetic radiation of such events might be detected by large surveys of AGNs (Graham et al. 2017; Cannizzaro et al. 2020).

Once a compact objects align with the disc, it can form a restricted three-body systems with two compact objects moving around the central supermassive black hole (SMBH) in closely packed circular orbits. The orbits of these restricted three-body systems may be unstable, leading to close encounters and Jacobi captures (Goldreich et al. 2002; Gondán & Kocsis 2021; Boekholt et al. 2022). When the

* E-mail: dearye@mail.ustc.edu.cn(YL)

† E-mail: yfyuan@ustc.edu.cn(YFY)

separation of two compact objects is smaller than a critical radius, known as the Hill radius or Jacobi radius, where the gravitation force between two compact objects is comparable to the tidal force of the central SMBH, the evolution of system turns to chaos and close encounters and Jacobi captures become possible. During the close encounters, the two compact objects may dissipate a sufficient amount of energy to become a bound binary in the tidal field of the central SMBH. Jacobi capture is an efficient channel for binary BHs formation in AGN discs (Boekholt et al. 2022).

However, the formation of binary WDs via gravitational wave emission is difficult. The physical radius of WDs is around $\sim 10^4$ km, which is three orders of magnitude larger than the Schwarzschild radius of stellar massive BHs. During the close encounter of two WDs, the separation for strong gravitational emission is much smaller than the physical radius of WDs. What happens in a close encounter is therefore the collision of two WDs rather than the formation of a binary WDs. These white dwarf collisions, which could produce the type Ia supernovae (Rosswog et al. 2009; Raskin et al. 2009; Hawley et al. 2012), have been studied in field hierarchical systems (Hamers 2018) and globular clusters (Raskin et al. 2010). Compared with these environment, the high-density of WDs in AGN discs makes the WD-WD collisions happen.

In this work, we focus on the WD-WD collisions in the restricted three-body systems. Such systems consist with two WDs orbiting around a central SMBH; the separation between two WDs orbits is of the order of mutual Hill radii. Since the system is dynamically unstable, the two WDs may collide during the close encounters. We perform a series of N -body simulations to study the closest separation and WD-WD collisions in close encounters. Each set of simulations has different initial parameters: the initial orbital separation, the relative orbital inclination, and the mass of the central SMBH. The effect of different initial orbital radius is also considered.

The rest of the paper is organized as follows. In Section 2, we describe our analytical framework and initial numerical setups. In Section 3, we present the distribution and time evolution of closest separation between WDs and the fraction of WD collision. Finally, the main conclusions and discussion are summarized in Section 4.

2 METHODS

A large population of WDs is expected to be embedded in AGN accretion discs as a result of stellar evolution and dynamical friction. Such WDs finally circulate around the central SMBH with close orbits, due to the alignment and migration of WDs. Whilst WDs have close circular orbits, they may experience very close encounters, during which collision can happen. These direct collision between two WDs may lead to type Ia supernovae (Hamers 2018; Raskin et al. 2010; Grishin et al. 2021).

As the WDs align with the discs, gas torques might cause the WD orbits to change over time as they undergo the so called type I migration within the discs. The type I migration timescale (Tanaka et al. 2002; Paardekooper et al. 2010; McKernan et al. 2012, 2018) can be estimated as

$$t_{\text{mig}} \approx 7.9 \text{ Myr} \left(\frac{N}{3} \right)^{-1} \left(\frac{r}{100 r_g} \right)^{-\frac{1}{2}} \left(\frac{m}{0.6 M_\odot} \right)^{-1} \times \left(\frac{h/r}{0.01} \right)^2 \left(\frac{\Sigma}{10^5 \text{ kg m}^{-2}} \right)^{-1} \left(\frac{M}{10^6 M_\odot} \right)^{\frac{3}{2}}, \quad (1)$$

where m and M are the mass of the WD and the central SMBH respectively, r is the semi-major axis of WD, r_g is the gravitational

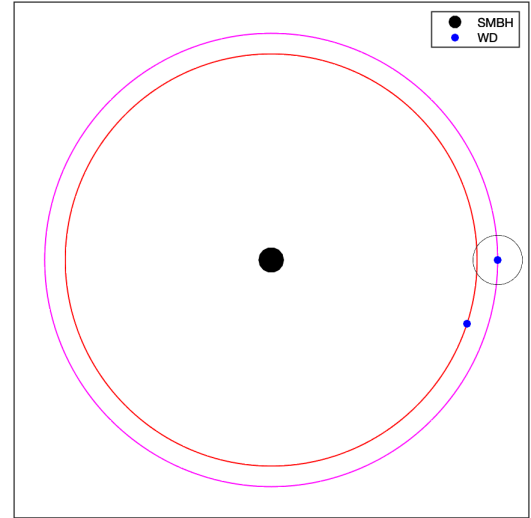


Figure 1. Picture of the simulation system. The system consist with a central SMBH (black dot) and two WDs (blue dot). The two WDs orbit on nearly circular and nearly co-planer orbits around the SMBH.

radius, defined as GM/c^2 , Σ is the surface density of the disc, h/r is the disc aspect ratio, and N is a numerical factor of the order of 3. The lifetime of AGN disc is around 10 Myr. For a dense Sirko & Goodman (Sirko & Goodman 2003) model disc with $M = 10^8 M_\odot$, a WD migrate to $100 r_g$ in ~ 2.5 Myr (McKernan et al. 2020a). Consequently, it is possible for a WD to migrate to the inner AGN discs. In addition to the type I migration, WDs can also exist in inner AGN discs if those WDs align with the discs at small orbits. As the WDs migrate inward, they finally collect in the migration trap, where the net torque on a migrator is zero (Bellovary et al. 2016). Due to their different radii of alignment, migration rate, and their collection in the migration trap, WDs may have very close orbits in the AGN discs.

We consider a system consisting with a central SMBH, orbited by two WDs in nearly circular and nearly co-planer orbits (see Figure 1). Due to their alignment (Yang et al. 2019b; Fabj et al. 2020) and migration (Tanaka et al. 2002; Paardekooper et al. 2010), the orbits of the two WDs may be very close to each other. In this paper, we set the central SMBH mass as M , the two WDs masses as m_1, m_2 , and the initial semi-major axis around the SMBH as a_1, a_2 . We define $p = a_2 - a_1$ to be the initial orbital separation. Different initial semi-major axis cause the two WDs to have slightly different orbital periods. In consequence, their relative separation gradually decreases with time. If their initial orbital separation p is much larger than their mutual Hill radius, their orbits are still stable. If their initial orbital separation p is of the order of their mutual Hill radius, their orbits might become unstable and the subsequent evolution become chaotic. Here, the mutual Hill radius is defined as

$$R_H \equiv \frac{a_1 + a_2}{2} \left(\frac{m_1 + m_2}{3M} \right)^{1/3} \approx a_1 \left(\frac{m_1 + m_2}{3M} \right)^{1/3}. \quad (2)$$

If we ignore the influence of the disc, the boundary between "stable" and "unstable" gives as a critical orbital separation p_c (Gladman 1993)

$$p_c = 2 \cdot 3^{1/6} \left(\frac{m_1 + m_2}{3M} \right)^{1/3} = 2\sqrt{3} R_H. \quad (3)$$

While $p < p_c$, the orbital evolution will become chaotic and Jacobi captures start to play an important role during the close encounters.

As a result, the closest separations of the two WDs can reach small values during close encounters. The bonding energy of a stable binary WD at the Hill radius is given by

$$E_b = \frac{Gm_1m_2}{2R_H}. \quad (4)$$

At the closest separation, the energy dissipation by gravitational wave emission can be given by (Peters 1964; Turner 1977)

$$\Delta E_{GW} = \frac{85\pi}{12\sqrt{2}} \frac{G^{7/2}(m_1m_2)^2(m_1+m_2)^{1/2}}{c^5 r_p^{7/2}}, \quad (5)$$

where r_p is the closest separation of the two WDs. If we neglect the possible effect of tidal dissipation and gas drag, the gravitational wave emission is the only mechanism to dissipate energy between two WDs. To form a stable binary WD, we need $\Delta E_{GW} \gtrsim E_b$ (Li et al. 2022), i.e.

$$r_p \lesssim r_b \equiv 3.48 \left(\frac{m_1m_2}{(m_1+m_2)^2} \right)^{2/7} \left(\frac{m_1+m_2}{M} \right)^{10/21} \left(\frac{GM/c^2}{a_1} \right)^{5/7} R_H. \quad (6)$$

Therefore, we can probe for a critical separation value of r_b , below which a bonding binary WD can be formed by gravitational wave emission with given M and a_1 . To eject one of the two WDs from the system during close encounters, we require

$$\frac{Gm_1m_2}{r_e} \gtrsim \frac{1}{2} \frac{m_1m_2}{m_1+m_2} v_{\text{orb}}^2 \quad (7)$$

where r_e is the ejection separation and v_{orb} is the orbital velocity, $v_{\text{orb}} = \sqrt{GM/a_1}$. For two WDs with mass $m_1 = m_2 = 0.6M_\odot$, we define the direct WD-WD collision separation as the sum of the physical radii of the WDs, $r_c = 2r_{\text{WD}}$, which is approximate 1.5×10^7 m. If $M = 10^6M_\odot$, $a_1 = 100GM/c^2$, we find a critical gravitational wave bonding radius $r_b \lesssim 1.76 \times 10^5$ m, which is much smaller than the direct collision separation $r_c \approx 1.5 \times 10^7$ m. The ejection separation $r_e \lesssim 3.6 \times 10^5$ m. The two WDs therefore collide together before they form a binary WD through the emission of gravitational wave or they might be ejected from the system. As a result, there are two possible outcomes for WD close encounters: (i) the two WDs experience a relatively soft close encounter and the orbits separate to "stable" orbits; (ii) The two WDs experience a very close encounter and collide with each other.

In our simulations, we adopt N-body units in which $G = 1$, central SMBH mass $M = 1$, the WD orbit $a_1 = 1$. So we can get the initial period $P_1 = 2\pi$. The WD masses in units of the mass of SMBH are $m_1 = m_2 = 6 \times 10^{-7}$ and $m_1 = m_2 = 6 \times 10^{-8}$ for SMBH masses of 10^6M_\odot and 10^7M_\odot respectively (i.e. $m_1 = m_2 = 0.6M_\odot$). We note that $r_g \approx 1.48 \times 10^9$ m and 1.48×10^{10} m for $M = 10^6M_\odot$ and 10^7M_\odot respectively, and the WD-WD collision separation is $r_c \approx 1.5 \times 10^7$ m. For convenience, we take the corresponding WD-WD collision separation to be $10^{-2}r_g$ and $10^{-3}r_g$ respectively. The initial orbital separation p is set to a series of values from $0.8R_H$ to $4.0R_H$. The two WDs orbits have initial eccentricities $e_1 = 0$, $e_2 = 10^{-5}$. The initial difference of the longitude is uniform distributed in the range $[0, 2\pi]$. The two WDs orbits may not be in the same plane. We define the inclination angle between the orbital plane and the disc plane as i_1 and i_2 . All details of the initial parameters are summarized in Table 1.

In this study, we integrate the three-body systems using the N-body code REBOUND (Rein & Liu 2012) with the IAS15 integrator (Everhart 1985; Rein & Spiegel 2015). For each individual simulation, we run $10^5 P_1$.

Table 1. The initial input parameters. The square bracket represent the uniform distribution between the two value in square bracket. Column 1 is the run name. Column 2 is the mass of SMBH in N-body units. Column 3 is the mass of WDs in N-body units. The two WDs have equal mass. Column 4 is the initial orbit radius in N-body units. Column 5 shows the initial orbital separations and Column 6 the number of samples.

name	M	m_1, m_2	a_1	p/R_H	i_1, i_2	N
Run1	1	6×10^{-7}	1	1.0	0	1000
Run2	1	6×10^{-7}	1	1.5	0	1000
Run3	1	6×10^{-7}	1	2.0	0	1000
Run4	1	6×10^{-7}	1	2.5	0	1000
Run5	1	6×10^{-7}	1	3.0	0	1000
Run6	1	6×10^{-7}	1	3.5	0	1000
Run7	1	6×10^{-7}	1	[0.8,4]	0	4000
Run8	1	6×10^{-7}	1	3.0	$ i_1 - i_2 = 10^{-3} \frac{R_H}{a_1}$	1000
Run9	1	6×10^{-7}	1	3.0	$ i_1 - i_2 = 10^{-2} \frac{R_H}{a_1}$	1000
Run10	1	6×10^{-7}	1	3.0	$ i_1 - i_2 = 10^{-1} \frac{R_H}{a_1}$	1000
Run11	1	6×10^{-7}	1	3.0	$ i_1 - i_2 = \frac{R_H}{a_1}$	1000
Run12	1	6×10^{-8}	1	3.0	0	1000
Run13	1	6×10^{-9}	1	3.0	0	1000

3 RESULTS

In this section we present our simulation results with different initial parameters. In the following analysis, we consider the different initial orbital radius a_1 with physics values rather than N-body units. We record the first time at which the separation between two WDs is smaller than r_c as the collision time. In Section 3.1 we present the closest separation between two WDs and WD-WD collisions as a function of the initial orbital separation. In Section 3.2, we show the influence of the relative orbital inclination on system close encounters and WD-WD collisions, and consider the mass of the central SMBH in section 3.3. Finally, the event rate of the WD-WD collision in AGN discs is discussed in Section 3.4.

3.1 Closest separation and WD-WD Collisions

The close encounter criterion in this work is that the separation between WDs should be much less than the initial orbital separations, i.e. $\Delta r = |\mathbf{r}_1 - \mathbf{r}_2| \lesssim 10^{-1} p$. Here we consider the close encounters between two WDs in different initial orbital separation: the closest separation and collisions. WD-WD collision occurs when the closest separation is smaller than the WD-WD collision separation. We also discuss the WD-WD collision fraction at different initial orbit a_1 .

In Fig. 2, we plot the resulting closest separation in Run1-Run6. The blue crosses correspond to simulation samples with the given initial parameters. The red dotted lines show the initial orbital separation. Equation (3) gives the boundary between dynamically "stable" and "unstable" regions, criterion $p_c = 2\sqrt{3}R_H$. For $p = 3.5R_H > 2\sqrt{3}R_H$ in Run6, the closest separation is slightly smaller than the initial orbital separation and there are no close encounters. Conversely, Run2-Run5 with the unstable orbits undergo close encounters, and the closest separation is much smaller than

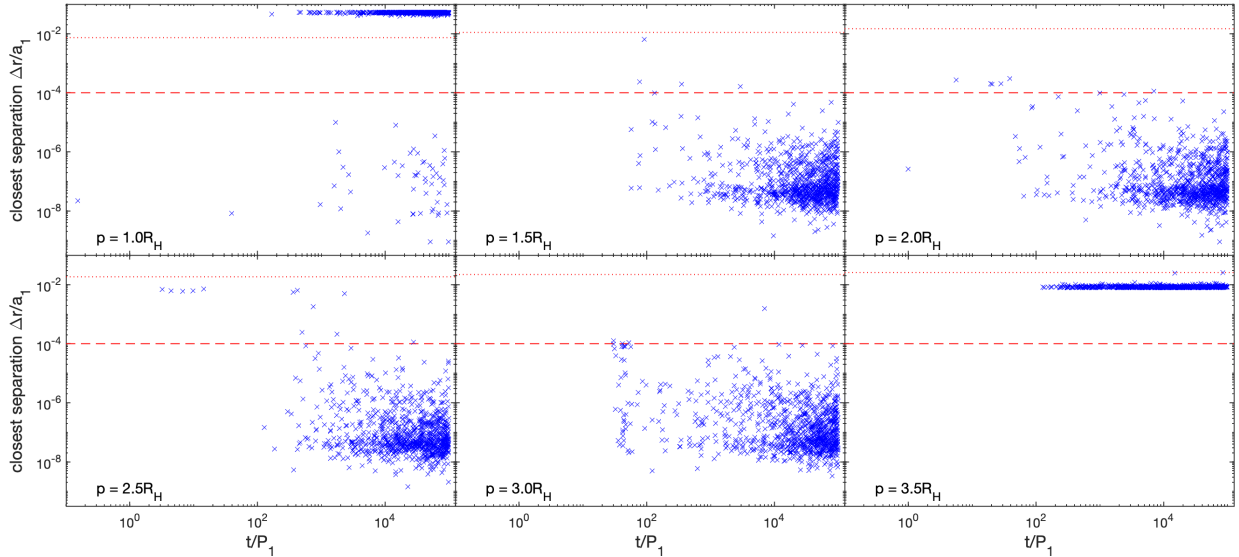


Figure 2. The closest separation between two WDs as a function of time at the closest separation. The blue crosses are individual simulation run. The initial orbital separation is $p = 1.0, 1.5, 2.0, 2.5, 3.0, 3.5R_H$. There are 1000 runs for every p . The red dashed line indicate the WD-WD collision separation with $a_1 = 100r_g$. The red dotted lines represent $p = \Delta r$.

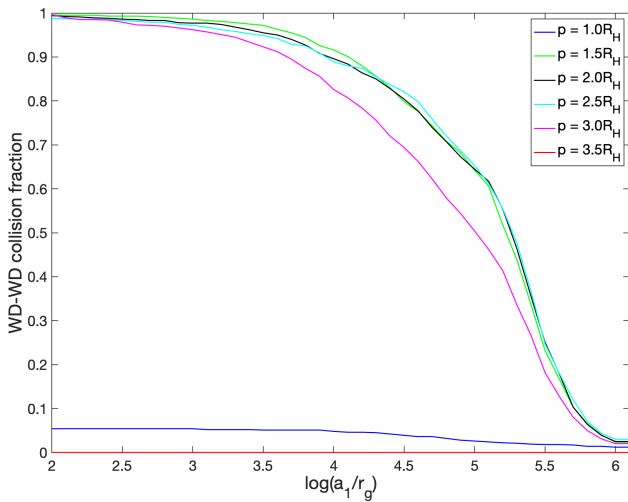


Figure 3. The WD-WD collision fraction as a function of initial WD orbital semi-major radius a_1 . Different colors correspond to the different initial orbital separation plot in Figure 1. We can see that the WD-WD collision fraction decrease as the a_1 increase. For $p = 3.5R_H$ and $p = 1.0R_H$, the collision fraction is much smaller than others, and there is no WD-WD collision for $p = 3.5R_H$.

the initial orbital separation. Run1 also have "unstable" initial orbital separation, but only around 5 per cent of samples undergo close encounters. The red dashed line corresponds to a WD-WD collision separation corresponding to $a_1 = 100r_g$. We see that WD-WD collisions occurred in nearly all samples for $p = 1.5, 2.0, 2.5, 3.0R_H$, but only a small part for $p = 1.0R_H$, and no collision occurred for $p = 3.5R_H$.

We can define the WD-WD collision separation in units of a_1 . The relative collision value r_c/a_1 decreases as a_1 increases. As a result, the collision fraction decreases. Fig. 3 shows the collision fraction in cases with different initial orbit a_1 . For $p = 3.5R_H$, which means stable orbit evolution, there is no collision occurring. While $p < p_c$, the WD orbits are unstable and the collision fraction decrease as

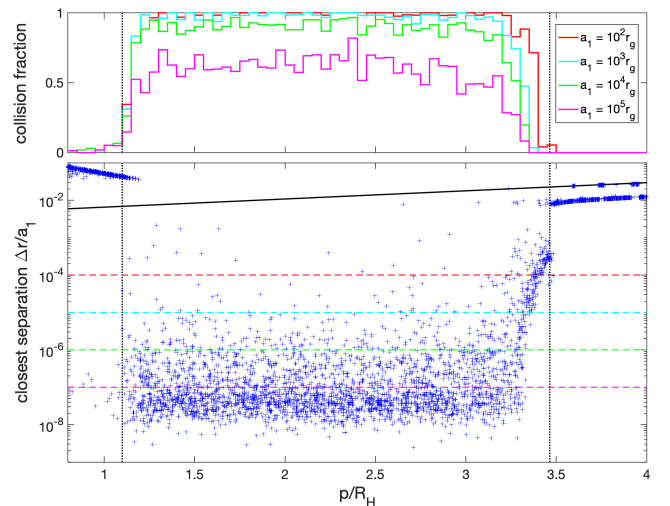


Figure 4. Upper panel: WD-WD collision fraction as a function of initial orbital separation at a given initial orbit a_1 . Different color correspond to different initial a_1 . **Bottom panel:** closest separation as a function of initial orbital separation. The brown dotted line corresponds to $\Delta r = p$. The red, cyan, green and magenta dashed line are the WD-WD collision separation of $a_1 = 10^2, 10^3, 10^4, 10^5r_g$ respectively. The black dotted line is the boundary between "stable" and "unstable" $p_c = 2\sqrt{3}R_H$.

a_1 increase. As the initial orbit a_1 changes, the WD-WD collision fraction decreases slowly at $a_1 < 10^4r_g$, but when $a_1 > 10^4r_g$ the WD-WD collision fraction decreases quickly to 50 per cent at 10^5r_g and 2 per cent at 10^6r_g . From Equation (7), it can be seen that, at the orbital radii $a_1 \geq 10^4r_g$, the ejection radius $r_e \approx 3.6 \times 10^7 \text{ m} > r_c$, which means one of the WDs may be ejected before they collide. In Run1, only 5 per cent of all samples show the WD-WD collision for $p = 1.0R_H$, the reason will be given next.

Fig. 4 shows the closest separation and WD-WD collision fraction in Run7 ($p/R_H \in [0.8, 4]$). The bottom panel plots the closest separation as a function of initial orbital separation. The black dotted

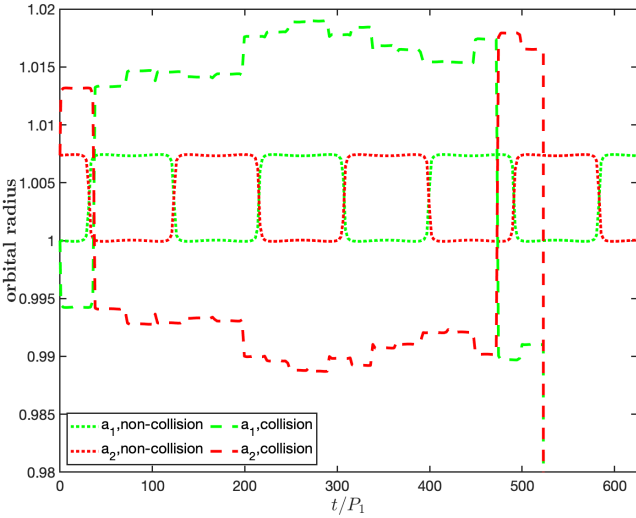


Figure 5. Orbits evolution of WDs at $p = R_H$. The dotted curves represent non-close encounter orbits and the dashed curves represent close encounter orbits. The color red and green correspond to a_1 and a_2 respectively.

line shows the result for $p = p_c$. The red, cyan, green and magenta dashed lines show the WD-WD collision separation for the cases $a_1 = 10^2, 10^3, 10^4, 10^5 r_g$ respectively. We find that almost all close encounters take place in the dynamical "unstable" region (i.e. $p < p_c$). However, WD-WD do not undergo a close encounter for $p < p_c$ in all samples. We can see that, at $p \lesssim 1.1R_H$, WD-WD close encounters become rarely, and most of the closest separation increases as the initial orbital separation decreases. The reason can be explained as follows. At small initial separation, the WDs are located on a horseshoe or a tadpole orbit in the rotating frame of reference. As they approach each other, one WD orbit decreases and another one increases, which leads to the exchange of their orbits. However, a few samples have also experienced close encounters, because their initial separation is very close, which lead to the initial orbit being outside the horseshoe orbit. Fig. 5 shows an example of the evolution of the orbital radius in the close encounter case and non-close encounter case for $p = R_H$. We can see that the two WDs exchange their orbits every time they encounter each other in the non-close encounter case, but in the close encounter case, the evolution of the orbits are chaotic and one WD is ejected in a very close encounter at around $520P_1$.

Fig. 6 shows the cumulative WD-WD collision fraction as a function of time in Run5 (i.e. $p = 3.0R_H$). The colored solid lines correspond to the results for the different initial orbital radii a_1 . The black dotted line represents the time $t = 62P_1$, which is twice the lowest common multiple of P_1 and P_2 . We find that, at the initial orbital radius $a_1 = 10^2 r_g$, WD-WD collisions occur in almost all samples. As the initial orbital radius increases, the WD-WD collision fraction decrease. For instance, in the case of $a_1 = 10^5 r_g$, only half the samples in our runs show WD-WD collisions. For the WD-WD collision samples, around 70 per cent of WD-WD collisions occur during the first two encounters (i.e. $t < 62P_1$) for $a_1 = 10^2 r_g$, but only 30 per cent at $t > 62P_1$. As the orbital radii increase, WD-WD collisions occurring during the first two encounters decrease sharply.

Due to the type I migration of WDs, the orbital radii will decrease. The time-scale of type I migration can be estimated from equation (1). Here we simply estimate the WD-WD collision timescale as $t_c = 10^5 P_1 / f_c$, where f_c is the cumulative WD-WD fraction in $10^5 P_1$. In the outer region ($r \gtrsim 10^5 r_g$) of the discs, the type I migration time-

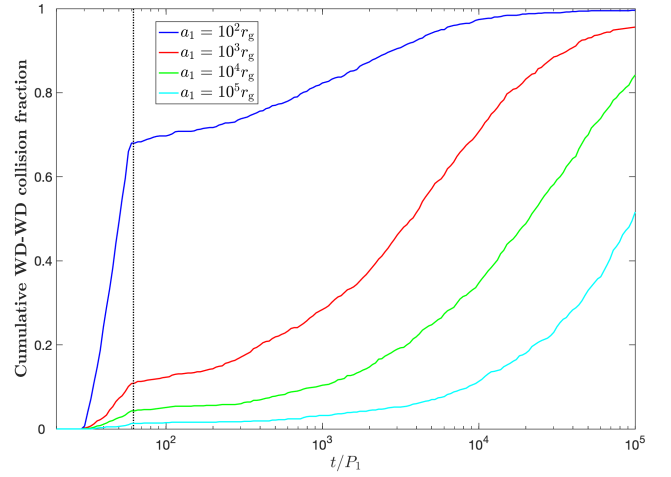


Figure 6. The cumulative WD-WD collision fraction distribute as a function of simulation time for Run5. The colored curves correspond to the initial orbit radius $a_1 = 10^2, 10^3, 10^4, 10^5 r_g$ respectively. The black dotted line represents time $t = 62P_1$.

scale is smaller than the WD-WD collision timescale, i.e. $t_{\text{mig}}(r) \lesssim t_c(r)$, which means the two WDs may migrate to the inner region ($r < 10^5 r_g$) before they collide. The large ejection separation in the outer region may lead to one of the WDs being ejected from the system, which can also decrease the rate of WD-WD collision. In conclusion, WD-WD collisions mainly occur in the inner region ($r < 10^5 r_g$) of the discs; they are rare in the outer region because most of the WDs have migrated into the inner region or been ejected when they collide.

3.2 Results with initial inclinations

The existence of an initial relative orbital inclinations can affect the orbital separation between two WDs. Assuming that two WDs have a small relative inclination $\Delta i = |i_1 - i_2|$, the orbital distance at the same longitude is larger than that without inclination. Naturally, we expect a decrease in close encounter fraction as the relative inclination Δi increases. Consequently, the closest separation becomes larger and the collision fraction will decrease. Run8 - Run12 are a series of simulations with the different inclinations.

Fig. 7 shows the distribution of probability of closest separation r_p between the two WDs. The upper panel shows the cumulative distribution and the bottom panel the probability density function. The colored lines correspond to results with different initial inclinations. We find that the peak of the closest separation for coplanar orbits is around $10^{-7.5} a_1$, and nearly all closest separation have $r_p \lesssim 10^{-5} a_1$. As the relative inclination Δi increases, the peak of the closest separation increases. For small relative inclination $\Delta i \lesssim 10^{-1} R_H / a_1$, almost all of the closest separation have $r_p \lesssim 10^{-4} a_1$. However, for $\Delta i = R_H / a_1$, around 20 per cent of the samples with closest separation $r_p > 10^{-4} a_1$.

Fig. 8 shows the cumulative WD-WD collision fraction as a function of time for the different relative inclinations. From the top panel to the bottom one, the initial orbital radius a_1 is set to be $10^2 r_g, 10^3 r_g$ and $10^4 r_g$, respectively. We find that, for the relative inclinations $\Delta i \lesssim 10^{-2} R_H / a_1$, the cumulative WD-WD collision fraction is almost the same as that in the case of coplanar orbits at $10^5 P_1$, but for large relative inclinations $\Delta i > 10^{-2} R_H / a_1$, the WD-WD collision fraction decreases quickly, and the larger the relative inclination, the

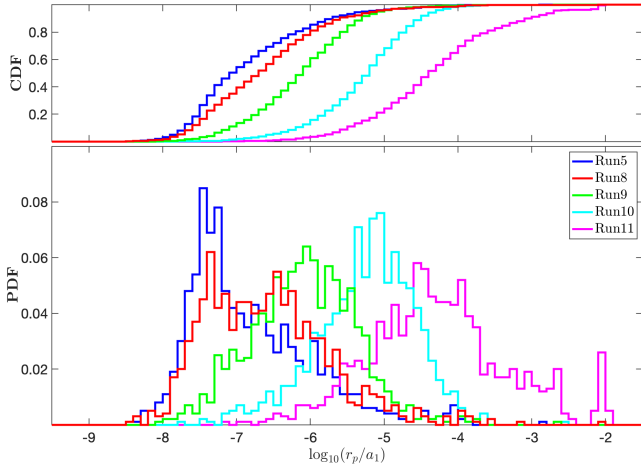


Figure 7. Probability density function of the closest separation between two WDs in close encounters. The colored curves correspond coplanar orbits (blue curve), $\Delta i = 10^{-3} R_H/a_1$ (red curve), $\Delta i = 10^{-2} R_H/a_1$ (green curve), $\Delta i = 10^{-1} R_H/a_1$ (cyan curve), and $\Delta i = R_H/a_1$ (magenta curve).

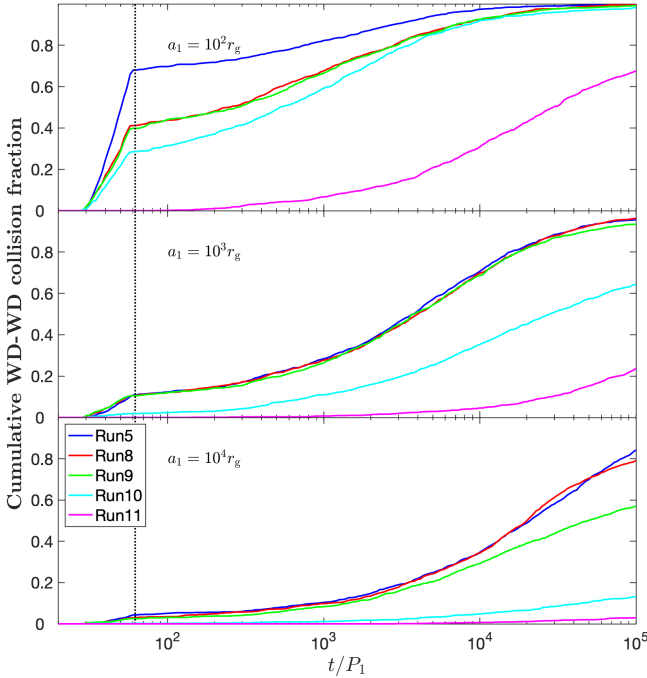


Figure 8. The cumulative WD-WD collision fraction as a function of time. From the top panel to bottom correspond to the initial orbital radius $a_1 = 10^2 r_g$, $10^3 r_g$, $10^4 r_g$. The colored curves correspond to different initial inclination given in Table 1. The black dotted line represents time $t = 62 P_1$.

faster the WD-WD collision fraction decreases. This indicates that small relative inclinations have nearly no effect on WD-WD collision, but large relative inclination can reduce the WD-WD collision rate sharply. There are almost no WD-WD collision for $\Delta i = R_H/a_1$ at all radius in the first $62 P_1$. However, for $\Delta i \lesssim 10^{-2} R_H/a_1$, the WD-WD collisions are considerable ($\gtrsim 10$ per cent) in the first $62 P_1$ for $a_1 \lesssim 10^3 r_g$. For $\Delta i = 10^{-1} R_H/a_1$, around 30 per cent of WD-WD collisions occur in first $62 P_1$ for $a_1 = 10^2 r_g$, but there are almost no WD-WD collisions for $a_1 \gtrsim 10^3 r_g$.

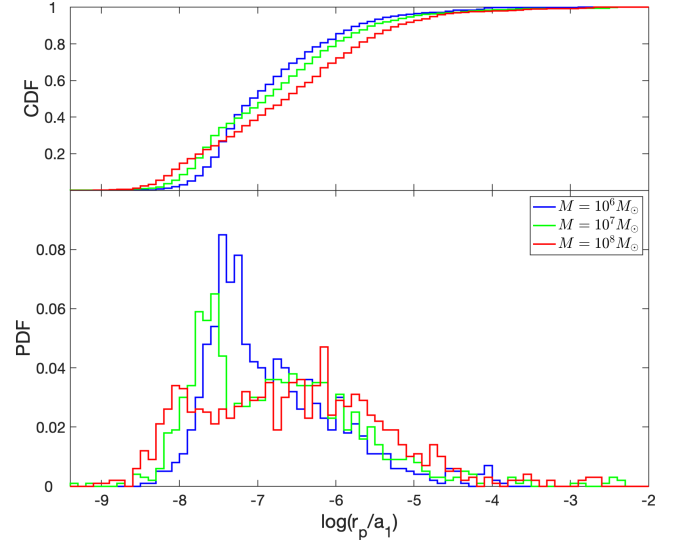


Figure 9. Upper panel: Cumulative closest separation distribution as a function of closest separation. Bottom panel: Probability distribution of closest separation as a function of closest separation. The blue, green and red curve correspond to the central SMBH mass $M = 10^6 M_\odot$, $10^7 M_\odot$ and $10^8 M_\odot$ respectively.

3.3 Results with the different mass of SMBH

The mass of the central SMBH can span several orders of magnitude. In Run13 and Run14, we investigate the effects of SMBH mass $M = 10^7 M_\odot$ and $10^8 M_\odot$, corresponding to mass ratio between WDs and SMBH of 6×10^{-8} and 6×10^{-9} respectively.

Fig. 9 shows the distribution of the closest separation as a function of time. The blue, green and red curves correspond to the results for SMBH masses $M = 10^6 M_\odot$, $10^7 M_\odot$ and $10^8 M_\odot$, respectively. We find that the cumulative closest separation distributions are very similar for the different SMBH mass, but the closest separation distribution for a more massive SMBH is more flat.

More massive SMBHs have larger r_g . This indicates that, at $a_1 = 10^2 r_g$, the ratio between WD-WD collision separation and the orbital radius (i.e. r_c/a_1) will decrease as SMBH mass increases. Fig. 10 shows the cumulative distribution of WD-WD collision at different initial radii for different SMBH masses. We find that, as expected, WD-WD collisions decrease as SMBH mass increases. Unlike $M = 10^6 M_\odot$, there are almost no WD-WD collisions during the first two encounters for $M = 10^7 M_\odot$ and $10^8 M_\odot$. At $a_1 = 10^4 r_g$, only ~ 10 per cent of samples have WD-WD collisions for $M = 10^8 M_\odot$. If we consider migration and $10^5 P_1 \approx 10 \text{ Myr}$ for $M = 10^8 M_\odot$ and $a_1 = 10^4 r_g$, the WD-WD collision fraction will be lower. As a result, WD-WD collisions in our model should occur preferentially in AGNs with less massive SMBHs.

3.4 WD-WD Collision rate

The number of BHs around the SMBH is about $\sim 1 - 4 \times 10^4$ (Gerozov et al. 2018). According to the stellar IMF (Kroupa 2001), the number of WDs are ten times larger than that of BHs. As a result, $\sim 2 \times 10^5$ WDs should exist around the central SMBH. We assume that the distribution of the stellar mass is cuspy and the initial number density of WDs is given as follow (Tagawa et al. 2021b),

$$\frac{dN_{\text{WD}}(r)}{dr} \propto r^{-0.5}, \quad (8)$$

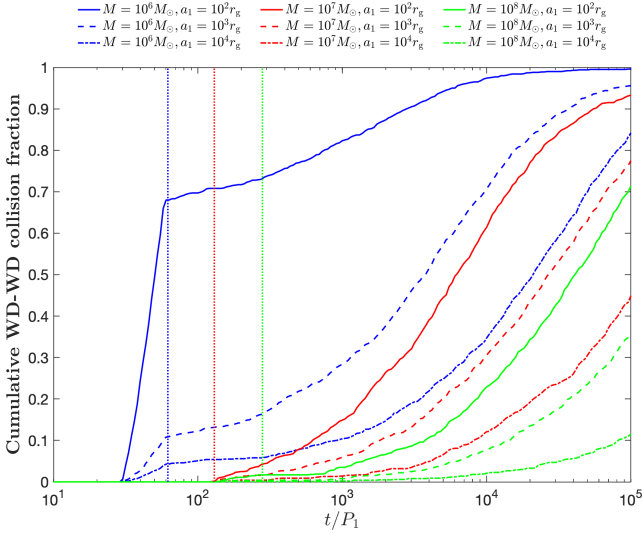


Figure 10. Cumulative WD-WD collision fraction as a function of time. The blue, red and green curves correspond to the results for $M = 10^6, 10^7, 10^8 M_\odot$ respectively. The solid curves represent $a_1 = 10^2 r_g$, the dashed curves represent $a_1 = 10^3 r_g$ and the dashed-dotted curves $a_1 = 10^4 r_g$. The dotted lines represent $t = 62 P_1$.

where $N_{\text{WD}}(r)$ is the total number of WDs within distance r from the SMBH.

Due to type I migration, the orbital separation between WDs will change with time. As their orbital separation reaches $\sim 3 R_H$, they will form a "SMBH+WD+WD" systems. For such a system, the WD-WD collision rate can be written as

$$\mathcal{R} = n_{\text{GN}} \times f_{\text{AGN}} \times \frac{N_{\text{WD}} \times f_d \times f_{3b} \times f_c}{\tau_{\text{AGN}}}, \quad (9)$$

where n_{GN} is the number density of galactic nuclei in the Universe, f_{AGN} is the fraction of galactic nuclei that have active AGNs, τ_{AGN} is the lifetime of AGNs, N_{WD} is the total number of WDs within distance $10^6 r_g$ from the central SMBH, f_d is the fraction of WDs that end up in AGN disc, f_{3b} is the probability of forming a three-body system, and f_c is the fraction of WD-WD collisions in such a three-body system. Our finding indicates that WD-WD collisions occur in nearly all samples at the inner region of the discs ($r < 10^4 r_g$) if we extend the simulation time to the AGN lifetime, but at the outer region of the disc ($a_1 > 10^4 r_g$) the WD-WD collision fraction will decrease quickly, especially for SMBHs with large mass. We therefore assume that, as the WDs migrate to $r < 10^4 r_g$, the WD-WD collision fraction $f_c = 1$, for other case $f_c = 0$. We also assume that, for all AGNs, half of the WDs in AGN discs can migrate to $r < 10^4 r_g$ and form restricted three-body systems, which gives $f_{3b} = 0.25$. Thus, we can get an approximately WD-WD collision rate

$$\mathcal{R} = 300 \text{Gpc}^{-3} \text{yr}^{-1} \frac{n_{\text{WD}}}{0.006 \text{Mpc}^{-3}} \frac{N_{\text{WD}}}{2 \times 10^5} \frac{f_{\text{AGN}}}{0.1} \frac{f_d}{0.1} \times \frac{f_{3b}}{0.25} \frac{f_c}{1} \left(\frac{\tau}{10 \text{Myr}} \right)^{-1}. \quad (10)$$

If all of those WD-WD collisions can produce type I SNe, we have an overall event rate $300 \text{Gpc}^{-3} \text{yr}^{-1}$ in AGN discs. The observed rate of type Ia SNe in the local universe is $2.5 \pm 0.5 \times 10^4 \text{Gpc}^{-3} \text{yr}^{-1}$ (Li et al. 2011; Cappellaro et al. 2015). Therefore, WD-WD collisions only constitute roughly 1 per cent of the observed rate of SN Ia.

There are some caveats and conditions that can influence our estimation of the event rate. First, there are uncertainties in the properties

of the AGNs and the distributions of WDs. The number of WDs in AGN discs likely depends on the mass density of discs and the distribution of WDs. For discs with large surface density Σ , the WDs more likely align with the discs (Yang et al. 2019b). In addition to the alignment, the migration of WDs is also affected by the surface density of the AGN discs and the mass of the central SMBHs. Around a more massive SMBH, such as $10^8 M_\odot$, the time-scale of the migration gets longer by a factor 10^2 (because $r_g = GM/c^2$) compared with the case of $10^6 M_\odot$, in which a WD starts at $R = 100 r_g$. In summary, migration-driven collisions more likely occur around less massive SMBHs. In the most semi-realistic disc models (Sirko & Goodman 2003; Thompson et al. 2005), the surface density Σ likely drops off at $\sim 10^3 r_g$ and h/R increases, leading to an increase in the time-scale of migration of WDs, but substantial changes of orbital radius can occur for WDs in the inner disc ($< 10^4 r_g$) over the lifetime of AGNs ($\sim 10 \text{Myr}$) (McKernan et al. 2012). At large radius ($> 10^4 r_g$), the migration of WDs into the inner disc might be less likely.

Second, in addition to migration, three additional factors are likely to be important in driving collisions of WDs. (i) Some WD binaries may exist that are formed through binary stellar evolution or dynamical process. Those WD binaries are likely to be dynamically hard in the nucleus, otherwise they might be ionized via dynamical encounters. Those hard WD binaries could be driven to merge via three-body scattering and due to the gas effects within the disc. (ii) If the turbulence scales of the discs are large enough (e.g. $> 2\sqrt{3}R_H$), WDs might not encounter each other due to the migration, but they might collide via random encounters. (iii) The dynamics might drive random encounters. WDs could collide randomly via direct collisions before they align with AGN discs. Even after they align with AGN discs, they might undergo random collisions during the damping of their eccentricity.

Third, other compact objects (BHs and NSs) and stars in AGN discs, neglected in this study, might influence WD-WD collisions. Since the migration rate for BHs and NSs in the AGN disc is fast, BHs and NSs will easily encounter WDs via fast migration and can tidally disrupt them during their close counters (Metzger 2012), which may decrease the population of WDs in the disc. In addition to encounters with compact objects, WDs can also encounter stars in the disc, and this might lead to the explosions of both stars.

4 CONCLUSION AND DISCUSSIONS

In this work, we study the closest separation between two WDs and WD-WD collisions via close encounters in AGN discs. We perform a set of N-body simulations with different initial parameters, including the initial orbital separation, the relative orbital inclination of the WDs, and different masses of SMBHs. According to our analysis and simulations, the WDs in AGN discs cannot form binary WD systems via the emission of gravitational wave. Our findings are as follows:

In Run1-Run7, the initial orbital separation changes from $0.8 R_H$ to $4.0 R_H$. It is found that close encounters between WD-WD only occur at $p \lesssim 2\sqrt{3}R_H$. For $1.1 R_H \lesssim p \lesssim 2\sqrt{3}R_H$, the closest separation between two WDs is concentrated between $10^{-8} a_1$ and $10^{-6} a_1$. As $p \lesssim 1.1 R_H$, most WDs enter horseshoe or tadpole orbits, which leads to fewer WD-WD close encounters (see Figs 4 and 5). In the case of $p = 3.0 R_H$, the WD-WD collision fraction decreases as the initial orbit radius a_1 (Fig. 3) increases. In the inner region of the disc ($r \lesssim 10^3 r_g$), considerable WD-WD collisions occur at $t < 62 P_1$ (Fig. 6). We note that WD-WD collisions in our systems can occur at $a_1 < 10^5 r_g$ for most of the samples within $10^5 P_1$.

Taking the relative orbital inclinations into consideration, the peak of the closest separation distribution increase as the relative inclinations increase (Fig. 7). For small relative inclinations (i.e. $\Delta i \lesssim 10^{-2} R_H/a_1$), the fraction of WD-WD collisions is almost the same as that in the case of coplanar orbits. However, for large relative inclinations (i.e. $\Delta i > 10^{-2} R_H/a_1$), the WD-WD collision fraction decreases quickly as the relative inclination increases and WD-WD collisions become rare at $a_1 \leq 10^4 r_g$ (Fig. 8).

It is clearly shown in Fig. 9 that the closest separation distribution is very similar in case of different SMBH mass. For more massive SMBHs, however, the ratio between collision separation and orbital radius is smaller, which leads to fewer events of WD-WD collisions for more massive SMBHs. For $M = 10^8 M_\odot$, there are nearly no WD-WD collisions at $a_1 = 10^4 r_g$ (Fig. 10). That means WD-WD collisions due to migration might happen preferentially in AGNs around less massive SMBHs.

According to our rough estimation, the event rate of WD-WD collisions is around $300 \text{Gpc}^{-3} \text{yr}^{-1}$. At most, such WD-WD collisions can contribute roughly 1 per cent of the overall event rate of Type Ia SNe. These SN explosions in AGN discs can generate strong shocks, which can lead to unique observations. In our following work, we will discuss the observational characteristics of SNe Ia in AGN discs resulting from WD-WD collisions.

A few uncertainties exist in our N-body simulations. The most important one is the effects of disc gas. During evolution, frictional disc forces can affect the dynamical evolution of WDs. (Li et al. 2022) have studied the effect of the disc forces with simple prescriptions; their results suggest that disc forces have little effect on the very close encounters. In addition to disc forces, WDs in AGN disc usually accrete gas. Nova reactions may exist on the surface of a WD as it accretes hydrogen from the AGN disc. The feedback of the nova could puff the gas off from the WD and influence the migration of the WD. Once the mass of WDs grow to the Chandrasekhar limit, WDs produce SN Ia. However, it is difficult for WDs to grow to the Chandrasekhar limit via accretion, because WDs are spun up more efficiently to reach the shedding limit before the Chandrasekhar limit (Pan & Yang 2021). Besides the growth of their mass, mini-discs around the WDs might help damp their orbital energy as they encounter each other and facilitate the formation of binary WDs (Li et al. 2023). Furthermore, accretion also affects the mass ratio of the two WDs. However, the masses ratio affects the close encounter rate by a factor of ~ 2 (Li et al. 2022). Thus, our results are roughly in keeping in systems with different mass ratio of WD-WD.

In this work, we study WD-WD collisions via close encounter in AGN discs. However, WD-BH, WD-NS and star-BH collisions also likely happen in AGN discs. In our following work, we will study close encounters of WD-BH, WD-NS and star-BH, which may lead to 'micro' Tidal Disruption Events (TDEs) and the subsequent light variation of AGNs (Perna et al. 2021; Grishin et al. 2021).

ACKNOWLEDGEMENTS

We would like to thank the referee for her/his critical comments which are very helpful for the improvement of this paper. YFY was supported by the National SKA Program of China No. 2020SKA0120300, and the National Natural Science Foundation of China (Grant No. 11725312). LCH was supported by the National Science Foundation of China (11721303, 11991052, 12011540375) and the China Manned Space Project (CMS-CSST-2021-A04, CMS-CSST-2021-A06). JMW acknowledges support from the National Science Foundation of China (NSFC-11833008 and -11991054) and

from the National Key R&D Program of China (2016YFA0400701). The numerical calculations in this paper have been done on the supercomputing system in the Supercomputing Center of University of Science and Technology of China.

DATA AVAILABILITY

The data underlying this article will be shared on reasonable request to the corresponding author (YFY).

REFERENCES

- Abbott B. P., et al., 2019, *ApJ*, **882**, L24
 Abbott R., et al., 2021, *ApJ*, **913**, L7
 Anninos P., Fragile P. C., Olivier S. S., Hoffman R., Mishra B., Camarda K., 2018, *ApJ*, **865**, 3
 Bartos I., Kocsis B., Haiman Z., Márka S., 2017, *ApJ*, **835**, 165
 Bellovary J. M., Mac Low M.-M., McKernan B., Ford K. E. S., 2016, *ApJ*, **819**, L17
 Boehholt T. C. N., Rowan C., Kocsis B., 2022, arXiv e-prints, p. arXiv:2203.09646
 Cannizzaro G., et al., 2020, *MNRAS*, **493**, 477
 Cappellaro E., et al., 2015, *A&A*, **584**, A62
 Cheng K. S., Wang J.-M., 1999, *ApJ*, **521**, 502
 Dittmann A. J., Miller M. C., 2020, *MNRAS*, **493**, 3732
 Everhart E., 1985, in Carusi A., Valsecchi G. B., eds, *Astrophysics and Space Science Library* Vol. 115, IAU Colloq. 83: Dynamics of Comets: Their Origin and Evolution. p. 185, doi:10.1007/978-94-009-5400-7_17
 Fabj G., Nasim S. S., Caban F., Ford K. E. S., McKernan B., Bellovary J. M., 2020, *MNRAS*, **499**, 2608
 Fragione G., Leigh N. W. C., Ginsburg I., Kocsis B., 2018, *ApJ*, **867**, 119
 Gayathri V., Yang Y., Tagawa H., Haiman Z., Bartos I., 2021, *ApJ*, **920**, L42
 Generozov A., Stone N. C., Metzger B. D., Ostriker J. P., 2018, *MNRAS*, **478**, 4030
 Gladman B., 1993, *Icarus*, **106**, 247
 Goldreich P., Lithwick Y., Sari R., 2002, *Nature*, **420**, 643
 Gondán L., Kocsis B., 2021, *MNRAS*, **506**, 1665
 Graham M. J., Djorgovski S. G., Drake A. J., Stern D., Mahabal A. A., Glikman E., Larson S., Christensen E., 2017, *MNRAS*, **470**, 4112
 Grishin E., Bobrick A., Hirai R., Mandel I., Perets H. B., 2021, *MNRAS*, **507**, 156
 Gröbner M., Ishibashi W., Tiwari S., Haney M., Jetzer P., 2020, *A&A*, **638**, A119
 Haas R., Shcherbakov R. V., Bode T., Laguna P., 2012, *ApJ*, **749**, 117
 Hamers A. S., 2018, *MNRAS*, **478**, 620
 Hawley W. P., Athanassiadou T., Timmes F. X., 2012, *ApJ*, **759**, 39
 Ji S., et al., 2013, *ApJ*, **773**, 136
 Kashyap R., Haque T., Lorén-Aguilar P., García-Berro E., Fisher R., 2018, *ApJ*, **869**, 140
 Kawana K., Tanikawa A., Yoshida N., 2018, *MNRAS*, **477**, 3449
 Kroupa P., 2001, *MNRAS*, **322**, 231
 Li G.-P., 2022, *Phys. Rev. D*, **105**, 063006
 Li R., Lai D., 2022, arXiv e-prints, p. arXiv:2202.07633
 Li W., Chornock R., Leaman J., Filippenko A. V., Poznanski D., Wang X., Ganeshalingam M., Mannucci F., 2011, *MNRAS*, **412**, 1473
 Li J., Lai D., Rodet L., 2022, arXiv e-prints, p. arXiv:2203.05584
 Li J., Dempsey A. M., Li H., Lai D., Li S., 2023, *ApJ*, **944**, L42
 Liu B., Lai D., 2021, *MNRAS*, **502**, 2049
 McKernan B., Ford K. E. S., Lyra W., Perets H. B., 2012, *MNRAS*, **425**, 460
 McKernan B., et al., 2018, *ApJ*, **866**, 66
 McKernan B., Ford K. E. S., O'Shaughnessy R., Wysocki D., 2020a, *MNRAS*, **494**, 1203
 McKernan B., Ford K. E. S., O'Shaughnessy R., 2020b, *MNRAS*, **498**, 4088
 Metzger B. D., 2012, *MNRAS*, **419**, 827

- Paardekooper S. J., Baruteau C., Crida A., Kley W., 2010, *MNRAS*, **401**, 1950
- Pan Z., Yang H., 2021, *ApJ*, **923**, 173
- Perna R., Tagawa H., Haiman Z., Bartos I., 2021, *ApJ*, **915**, 10
- Peters P. C., 1964, *Phys. Rev.*, **136**, B1224
- Raskin C., Timmes F. X., Scannapieco E., Diehl S., Fryer C., 2009, *MNRAS*, **399**, L156
- Raskin C., Scannapieco E., Rockefeller G., Fryer C., Diehl S., Timmes F. X., 2010, *ApJ*, **724**, 111
- Rein H., Liu S. F., 2012, *A&A*, **537**, A128
- Rein H., Spiegel D. S., 2015, *MNRAS*, **446**, 1424
- Rosswog S., Kasen D., Guillochon J., Ramirez-Ruiz E., 2009, *ApJ*, **705**, L128
- Samsing J., et al., 2020, arXiv e-prints, p. [arXiv:2010.09765](https://arxiv.org/abs/2010.09765)
- Secunda A., Bellovary J., Low M.-M. M., Ford K. E. S., McKernan B., Leigh N. W. C., Lyra W., Sándor Z., 2019, *The Astrophysical Journal*, **878**, 85
- Secunda A., et al., 2020, *ApJ*, **903**, 133
- Sirko E., Goodman J., 2003, *MNRAS*, **341**, 501
- Stone N. C., Metzger B. D., Haiman Z., 2017, *MNRAS*, **464**, 946
- Tagawa H., Haiman Z., Kocsis B., 2020a, *ApJ*, **898**, 25
- Tagawa H., Haiman Z., Bartos I., Kocsis B., 2020b, *ApJ*, **899**, 26
- Tagawa H., Kocsis B., Haiman Z., Bartos I., Omukai K., Samsing J., 2021a, *ApJ*, **907**, L20
- Tagawa H., Kocsis B., Haiman Z., Bartos I., Omukai K., Samsing J., 2021b, *ApJ*, **908**, 194
- Tanaka H., Takeuchi T., Ward W. R., 2002, *The Astrophysical Journal*, **565**, 1257
- The LIGO Scientific Collaboration et al., 2021, arXiv e-prints, p. [arXiv:2108.01045](https://arxiv.org/abs/2108.01045)
- Thompson T. A., Quataert E., Murray N., 2005, *ApJ*, **630**, 167
- Turner M., 1977, *ApJ*, **216**, 610
- Wang Y.-Z., Fan Y.-Z., Tang S.-P., Qin Y., Wei D.-M., 2021a, arXiv e-prints, p. [arXiv:2110.10838](https://arxiv.org/abs/2110.10838)
- Wang J.-M., Liu J.-R., Ho L. C., Du P., 2021b, *ApJ*, **911**, L14
- Wang J.-M., Liu J.-R., Ho L. C., Li Y.-R., Du P., 2021c, *ApJ*, **916**, L17
- Yang Y., et al., 2019a, *Phys. Rev. Lett.*, **123**, 181101
- Yang Y., Bartos I., Haiman Z., Kocsis B., Márka Z., Stone N. C., Márka S., 2019b, *ApJ*, **876**, 122

This paper has been typeset from a $\text{\TeX}/\text{\LaTeX}$ file prepared by the author.